Journal of Medicinal and Nanomaterials Chemistry 3 (2022) 185-195

Journal of Medicinal and Nanomaterials Chemistry

Journal homepage: https://jmnc.samipubco.com/

Original Research Article

Accumulated surface on stationary target: A new approach in electrospinning jet bending instability studies

Shahrzad Rahmani*

Department of Chemical Engineering, Babol Noshirvani University of Technology, Shariati Ave, P.O.Box 47148-7116, Babol, Iran

ARTICLE INFORMATION

Received: 16 April 2022
Received in revised: 3 June 2022
Accepted: 5 June 2022
Available online: 29 June 2022

DOI: 10.48309/JMNC.2022.3.2

KEYWORDS

Electrospinning
Jet bending instability
Desing of experiments
Response surface
Statistical analysis

ABSTRACT

Bending instability is a significant reason for the success of the electrospinning process for decreasing the fiber's diameter to nanometer scales and a determining factor in final fiber morphology. Observation of electrospinning of different polymers revealed that electrospun fibers accumulate in a circular area with various diameters in the case of a stationary flat plate target. There is an idea that the diameter of accumulated surface (ASD) is controlled by bending instability, and there is a correlation between electrospun fiber diameter and ASD. In this study, the accumulation behaviors of Polystyrene (PS), Polymethyl methacrylate (PMMA), and coaxially electrospun fibers of PS-PMMA were evaluated concerning their ASD sizes, the rate of ASD's growth, and the correlation between ADS size and the final diameters. To determine the role of processing parameters on this behavior and the relationship between the ASD and final fiber diameter, some experiments were designed for three factors of voltage, flow rate, and tip to target distance for electrospun fiber diameters and ASD in PMMA electrospinning. Two polynomial equations were found (via regression). Then, the polynomial models statistically were analyzed and discussed. Scanning electron microscopy (SEM) and fluorescent microscopy were applied for morphological studies, and Image J were used for measuring the sizes. The results demonstrated that during the electrospinning, the ASD grew with the natural logarithm of time and so ended to a plateau (specific diameter), and after that, the upcoming electrospun fibers accumulated on the former ones. Moreover, bigger ASDs were accompanied by smaller electrospun fiber diameters.

Corresponding author, email: Rahmani.sh@nit.ac.ir (S. Rahmani).

Graphical Abstract

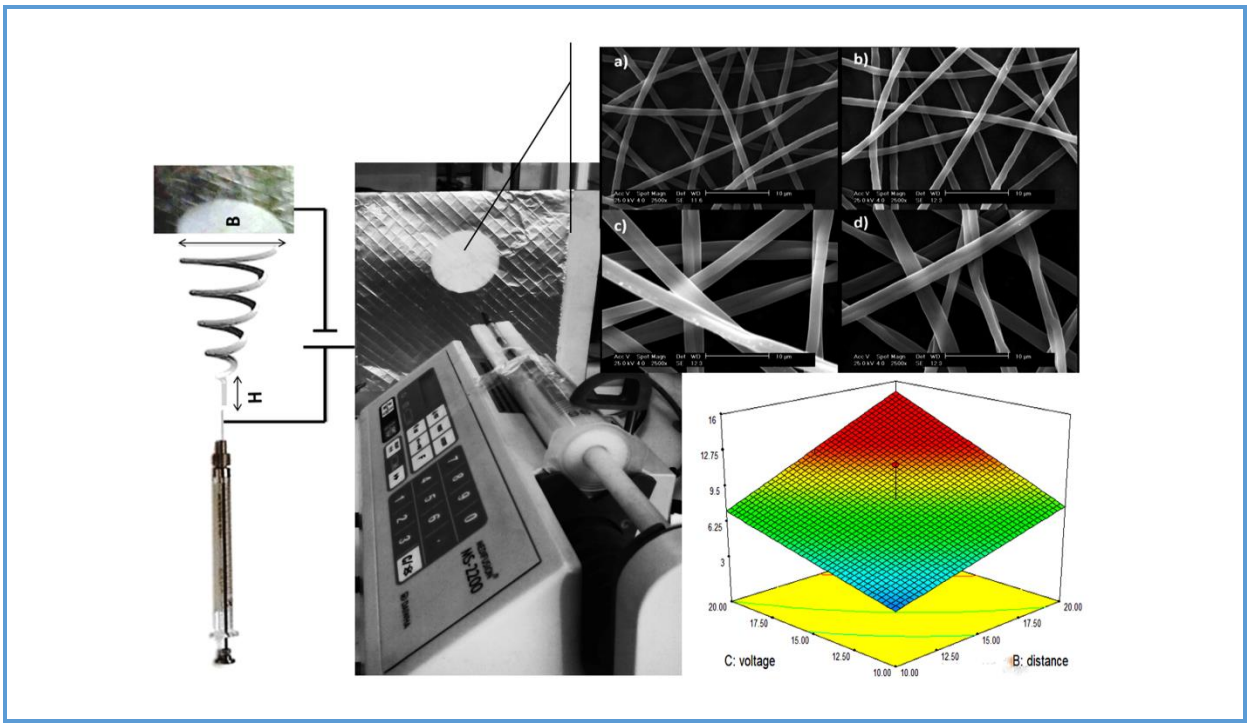

Introduction

Electrospinning is a facile and efficient method for producing nanofibers [1–3]. In this process, a viscous solution overcomes viscosity and surface tension by being drawn in an electric field from charged needle toward a grounded collector [4, 5]. It has been known that an electrospinning jet begins to bend after a short straight path due to repulsion of the same charges on every segment of the jet while the jet moves toward the collector. The bending also grows until it impinges on the collection. Meanwhile, the solvent evaporates, and the jet stretch to the narrower one, and finally, nanofibers accumulate on the collector. The severe stretching of the jet at the time of bending leads to fiber diameter size reduction to nanometers [1, 4].

Over the last few years, much research has been conducted on the electrospinning process to fabricate nanofibers for various applications [6–8]. The two categories of material (solvent selection, solution viscosity, conductivity, and polymer) and process parameters (voltage, tip to target distance, flow rate, ambient humidity, and temperature) are known as the main effective parameters of this process [1, 2, 9].

In our previous reports, this whipping and bending were simulated with a helical coil (i.e., a solenoid) whose base coil increases while the jet moves forward. So, the most oversized coil will be the one that hits the collector [4]. Hence, as much as bending expands, the collection area increases too. On the other hand, it can be said that, as much as bending expands, the jet stretches more, and the diameter of the electrospun fiber decreases. Ikuo *et al*. [10] found out the charge density, bending instability trajectory, and electrospinning jet diameter using high-speed camera observations, the electrified jet velocity measurements, and solving the equation of motion. In their study, the electric potential was calculated theoretically i.e., analysis of electric

field via finite element method. They believe their findings can be useful for new approaches in the electrospinning process [10].

Chi *et al*. [11] suggested a new scenario for the beginning of bending instabilities. In their study, the tip to target distance at a constant voltage was known to be effective on bending, extension rate, and diameter of electrospinning jet. In another study, Yu *et al.* [12] studied the jet bending instabilities from the perspective of solution conductivity. The solution conductivity was evaluated by adding salt to some solutions and comparing them with the neat ones. The results demonstrated that higher conductivity of solutions increases the Taylor cone, shortens the straight part, and enlarges the jet-end diameter [12].

Sailing *el al.* [13] predicted the whipping jet velocity by establishing the dynamic models in which the surface charge sets the velocity. They found that whipping jet velocity scales with motion time and the axial distance over an exponent of $-1/3$ and $-1/2$, respectively. They acclaimed that using their findings, the velocity and whipping jet stretching can be controlled more accurately, and the morphology of nanofibers can be designed [13].

Different polymers have been electrospun as yet. Polymethylmethacrylate (PMMA), a thermoplastic with excellent processability and environmental stability, has been a special polymer [14]. This polymer singly [15–18], in a blend with other polymers [17], and a composite with additives [19–21] has been electrospun. Also, the effects of some parameters, including solvent selection [22–25], viscosity and solution concentration, and molecular weight effects [24] on its electrospun fiber morphology and diameter size, have been discussed. There is also some research [25–28] on the effects of processing parameters.

This study aimed at investigating the factors that control this bending motion and the correlation between this bending and final fiber diameter. For this, polymers of PS, PMMA, and their core-shell coaxial fibers, were investigated. Since the largest coil was the one that reached the collector, the bending expansion of various polymers with time was investigated by measuring the diameter of the collection area with time. Afterward, experiments were designed and discussed using statistically investigated responses to study the effect of processing parameters.

Experimental

Materials and method

Polystyrene GPPS-1160 (from Tabriz petrochemical), Polymethyl methacrylate CM-205 (from Chi Mei Corporation, Taiwan), and dimethylformamide (from Merk) were used in this research. The solution was prepared by stirring 30 wt% of Polymers in DMF for 24 h in ambient conditions.

To electrospun the fibers, a high voltage power supply (Gamma High Voltage RR-60 model) was used to supply the electric field and a syringe pump (Medifusion Ms-2200) for pumping the solution at designed feed rates. The needle diameter was 0.7 mm. A grounded flat plate covered by aluminum foil was utilized as a collector. In the case of coaxial electrospinning, a coaxial needle was used instead and two pumps, one for feeding the core solution (PMMA) and the other for shell solution (PS). The final fiber was accumulated on the same flat plate. The electrospinning setup is illustrated in Figure 1.

The electrospun fiber's morphology and diameter were assessed using scanning electron microscopy (SEM XL30, PHILIPS) and ImageJ software.

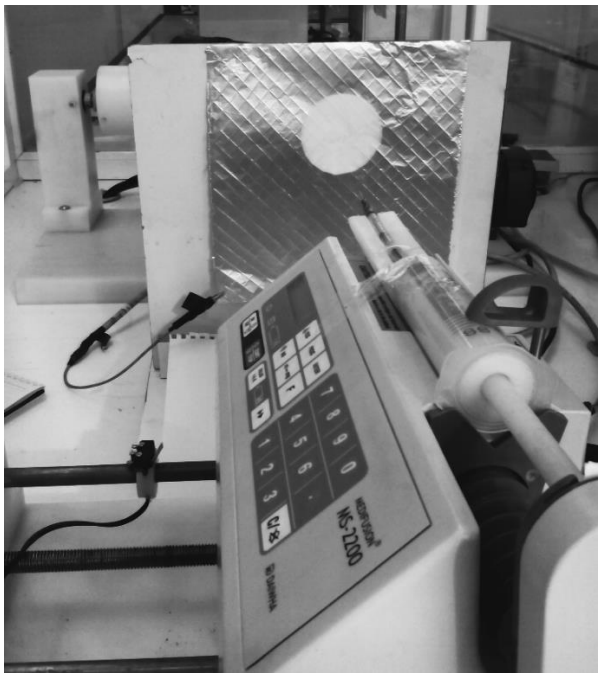

Figure 1. The electrospinning setup used in this study

Design export methods

The method of response surface (Central composite design) in one block and with three factors (each one with three levels) was carried out. The diameter of accumulated surface area on the target plate and electrospun fiber diameter was determined as the responses. Three factors of electrospinning voltage (kV), flow rate (mL/hr), and tip to target distance (cm) were the three processing factors under investigation (Table 1).

Results and Discussions

The accumulated area of PS electrospun fibers and PS-PMMA core-shell electrospun fibers are depicted in Figures 2a. As can be seen, both polymers gathered on a circular area have different area sizes while keeping the processing parameters at the same values. Any other polymer is also gathered on a stationary plate target in a circular area shape. As discussed before, this same circular accumulated area shape arose from the hitting of the last coins of the electrospinning jet bending to the target plate. Comparing Figures 2, this accumulation has the same shape in different polymers with different area sizes.

In Figure 3, the variation of accumulated area diameter is reported for PS, PMMA, and their core-shell fiber.

Table 1. Three factors and their levels in PMMA electrospinning investigation

Factors	Levels		
Voltage (kV)	10	15	20
Distance (cm)	10	15	20
Flow Rate (mL/hr)	0.25	0.5	1

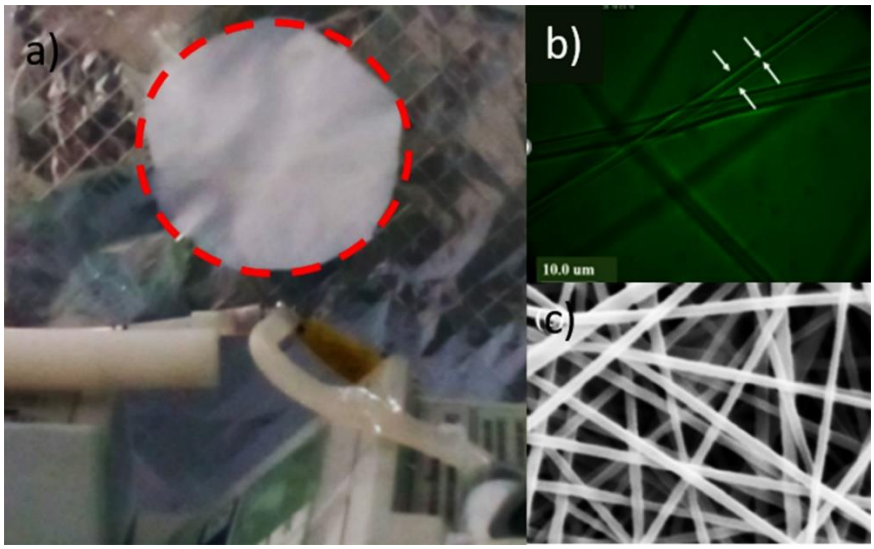

Figure 2. a) Circular accumulation of coaxially electrospun fibers of PS-PMMA on the flat plate, b) Fluorescent microscopic image of core-shell morphology of fibers, c) SEM images of electrospun PS-PMMA core-shell fibers

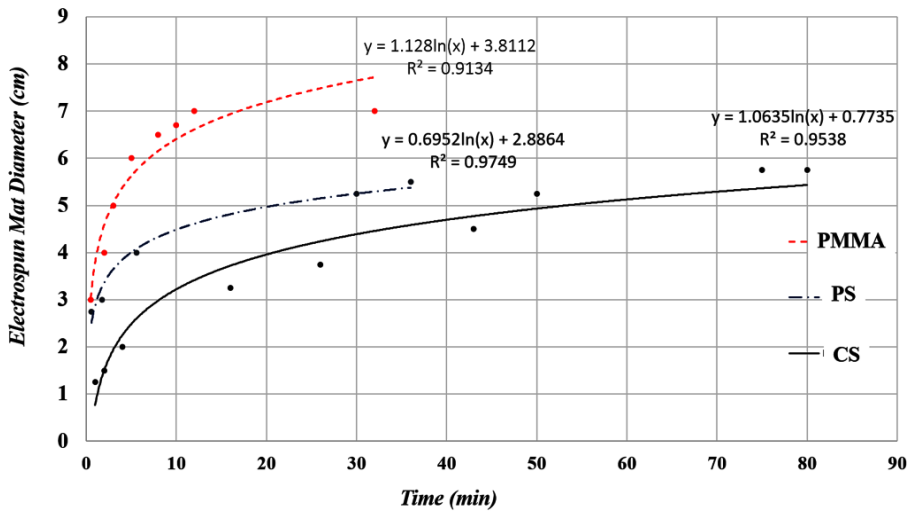

Figure 3. ASD growth rate with time for PS, PMMA, and PS-PMMA at the voltage of 15 kV, tip to target distance of 15 cm, and flow rates of 0.25 $^{\mu L}/_{hr}$ for each one of PS and PMMA electrospinning and an overall flow rate of 0.5 for core-shell electrospinning (each one of core and shell had a flow rate of 0.25 $^{\mu L}/_{hr}$)

Based on this plot, the growth of accumulation area (diameter) follows a natural logarithm relation with time, which ends in a plateau. Polystyrene and PS-PMMA core-shell fibers ensure the same ASD (about 5.5 cm), while PMMA ended at a plateau with an ASD of 8 cm, which is bigger than the others. PMMA and PS reached their ASD plateau after about 30 min

while this time was 80 min in the case of core-shell fibers. In other words, the ASD growth rate was the slowest one. The lagging behavior can be due to the coaxially electrospun jet's two times higher flow rate. Higher flow rates make more enormous Taylor cones and thicker jets. As much as the jet gets thicker, the charge density diminishes. As a result, not only does the jet experience lower electric forces, but also repulsions and bending decreases, and smaller ASD with thicker fibers will be produced. This can justify the smallest ASD of PS-PMMA coaxial electrospinning though this is not true about PS (i.e., PS with the same processing parameter as the PMMA's, had an ASD of 5.5, which was lower than PMMA's). Considering the same solution concentrations of PS and PMMA, one hypothesis that can explain the disparity between ASD of PS and PMMA is the potential difference between molecular weights of these two polymers.

On the other hand, inspire of different flow rates in PS electrospinning and PS-PMMA coaxial electrospinning led to the same ASD of 5.5 cm. However, the core-shell one was slower. This observation throws down the former interpretation. To get to a comprehensive explanation for these behaviors, more details and observations are needed.

The ASD dependency on the processing parameters was studied in PS electrospinning. These results are demonstrated in Figure 4 and Table 2. According to these results, ASD in PS electrospinning depends on voltage and tip to target distance. ASD enlarges as the voltage increases and distance decreases.

Table 2. Fitted equations and their R^2 on ASD[1] data for polymers

Polymer	Equation	R^2
PMMA	$ASD = 1.13\ln(t) + 3.8$	0.91
PS	$ASD = 0.69\ln(t) + 2.9$	0.97
PS-PMMA	$ASD = 1.06\ln(t) + 0.77$	0.95

[1] Accumulated Surface Diameter

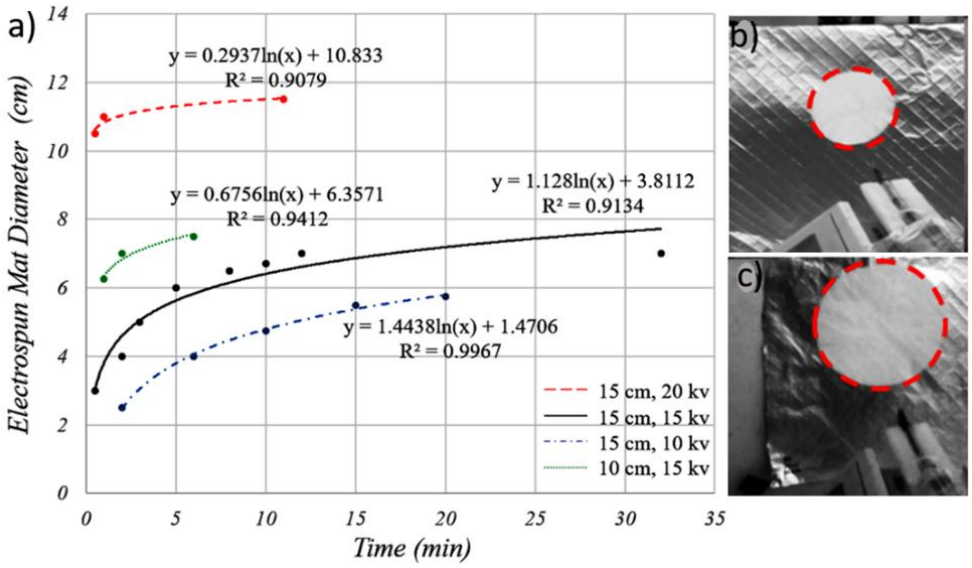

Figure 4. Electrospun fiber mat circular pattern accumulated on target at a) 10 kv, 15 cm, b) 20 kv, 15 cm

Figure 5 illustrates the SEM images of the PMMA fibers. In Figures 5**c** and **d**, the ribbon morphology of PMMA fibers can be seen. To face one number as the diameter for PMMA electrospun fibers, the cross-section of ribbon morphology was considered an ellipse with two axes. If the minor axis is codded with "a" and the major one with "b", the equivalent diameter which we used in our investigations was calculated from the equation of $r = \sqrt{a \times b}$.

The PMMA electrospinning was done based on the designed experiment with 3 factors of voltage, tip to target distance, and flow rates, each one at three levels. Then, after measuring the minor and major axes in the ellipsoidal cross-section of PMMA fibers, the equivalent radiuses were calculated and input as one of the responses. A non-transferred quadratic polynomial model was fitted on the responses with an R^2 of 0.95. The predicted versus actual values also verify the model's accuracy (Figure 6**a**). The three-dimensional surface response when the distance and voltage are variables is reported in Figure 6**b**. As seen in Figure 6, as much as the voltage and tip to target distance were increased, the diameter decreased. The reaction of reduction to amplification of voltage is because of severer electrospinning jet stretching in testified electric fields at higher voltages. Although increasing the distance decreases the electric field and should have led to bigger diameters, it seems that at higher distances due to jet path prolongation and the bending expansion overcomes, thus narrower fibers are produced.

ASD was the other response in our PMMA electrospinning study. A linear transferred model with Lamba of 0.76 was fitted on ASDs of PMMA. Box-Cox plot in Figure 7**a** shows the accuracy of lambda in the fitted model. The normal distribution of residuals and predicted versus actual values are also reported in Figure 7**b** and **c**, which verifies the model's suitability. Besides, the P-values are reported in Table 3. The model, voltage, and distance with P-values lower than 0.05 are known significant terms. Therefore, the linear response surface model can almost precisely represent the behavior of ASD at different voltages, distances, and flow rates. Moreover, distance and voltage are effective parameters on ASDs, while the flow rate variation cannot control or affectASD results.

As seen in Figure 8, electrospun fibers accumulated on bigger circles while both distance and voltage are at their highest values. Also, we can see the same trend in flow rate though based on its P-value, this term was not known as an efficient one. The results of ASDs are logical as we already knew that at higher voltages with intensified surface charges, instabilities and bending motions would develop. So the last coil would become more prominent. We can also say that at higher distances, jet coils grew more, and the last one would become bigger.

With more instabilities, longest jet path to the collector, and more intense stretching, it was expected that the accumulated fibers also become narrower, which was true in the case of higher voltages (Comparing Figures 6**b** and 7**b**). Figure 7**b** proves the bending amplification and ASD growth with increasing the distance, though the narrower fibers were found when the tip was placed closer to the target at the same voltages. This evidence bolds the dominance of electric field effect on fiber diameter versus bending instability.

According to Figure 9, there are no interactions between processing factors (voltage, distance, flow rate) on ASD in the selected range of this study.

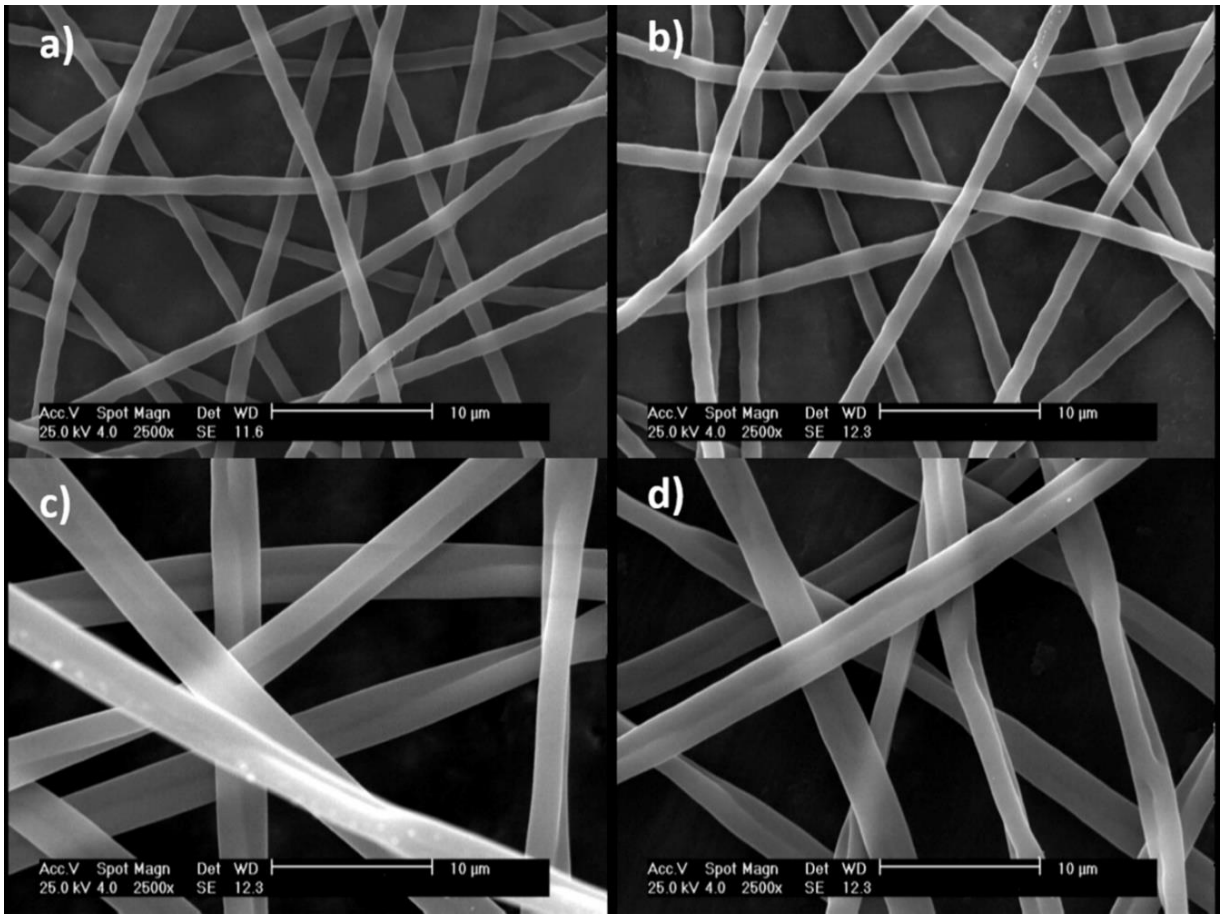

Figure 5. Electrospin fibers morphology at different processing parameter: a) 0.25 mL/h ,25 cm, 20 kV b) 0.5 mL/h, 20 cm, c) 10, 25, 92 d) 40, 10, 185

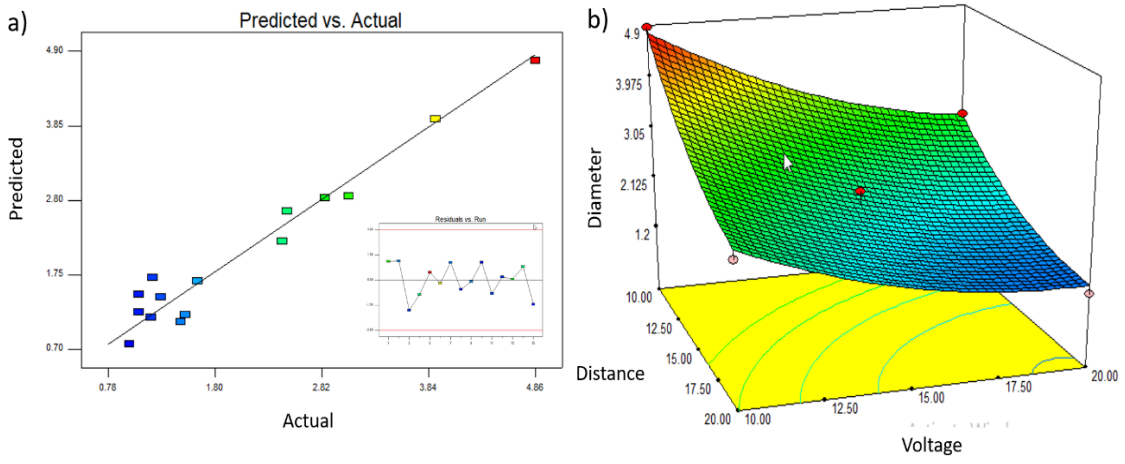

Figure 6. a) Predicted versus actual values, b) three-dimensional modeled surface on PMMA electrospun fiber diameters at different voltages and distances Table 3. Fitted equations and their R^2 on ASD[1] datas for polymers

Table 3. Fitted equations and their R^2 on ASD[1] datas for polymers

Term	P-values
Model	0.043
Voltage	0.034
Distance	0.0185
Flow rate	0.790

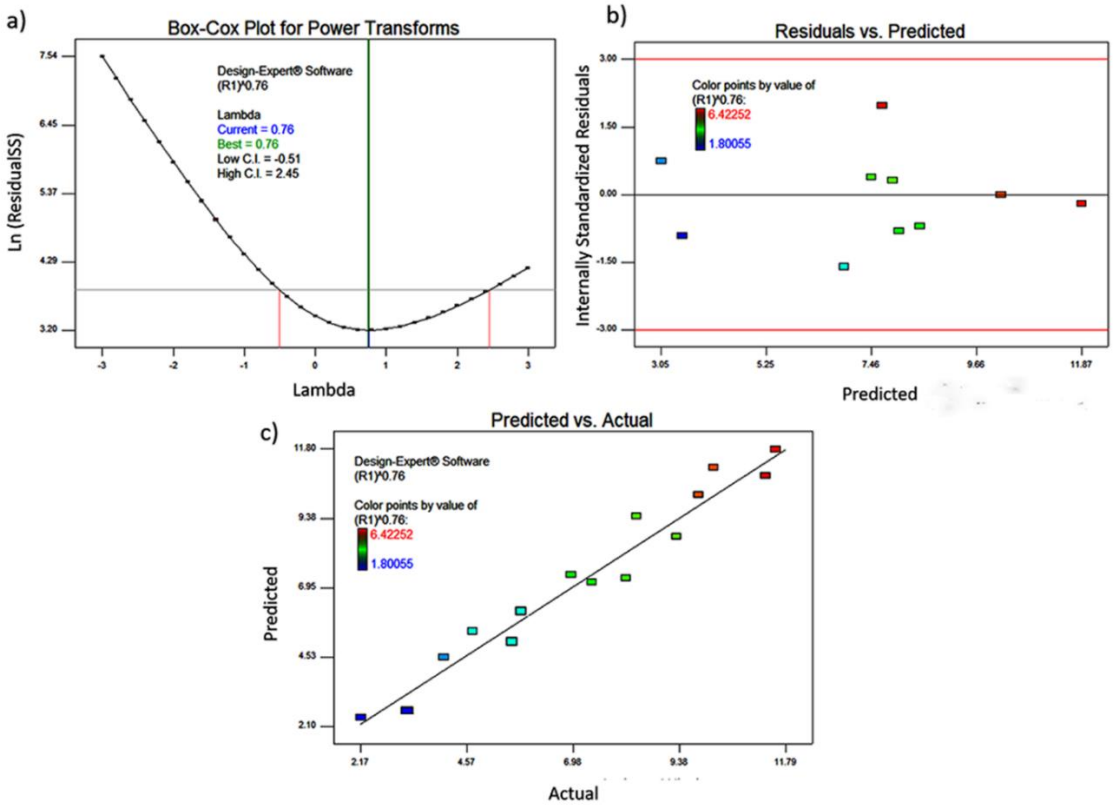

Figure 7. Diagnosis plots for PMMA electrospinning ASD fitted model. a) Box-Cox plot, b) residual versus predicted, and c) predicted versus actual values plots

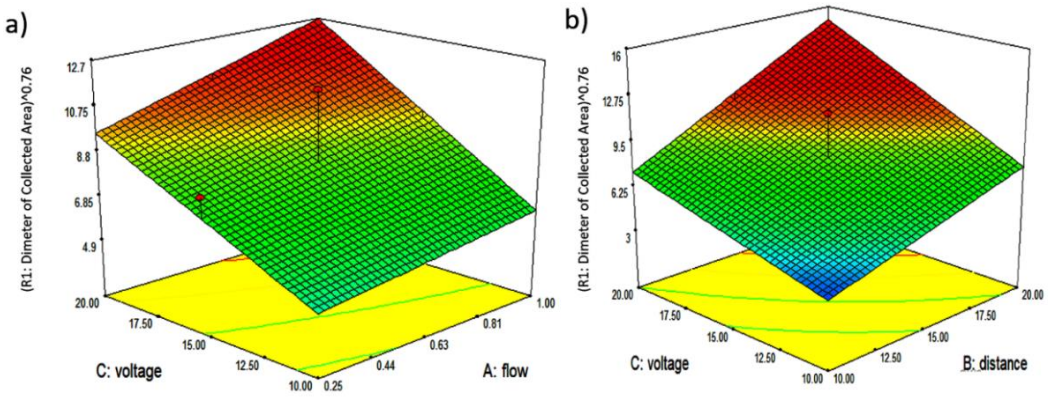

Figure 8. Three-dimensional surface responses of ASD versus a) voltage-flow rate and b) voltage-distance

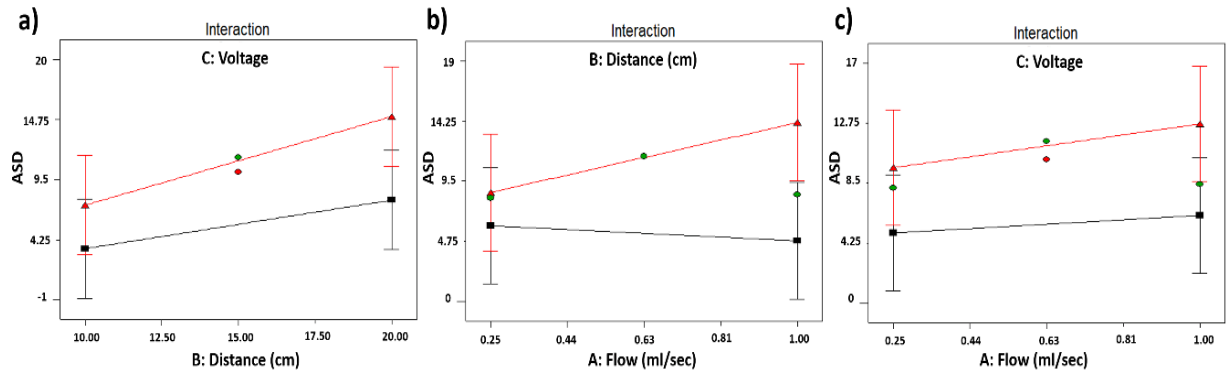

Figure 9. Interaction between processing factors on ASD a) voltage-distance, b) distance-flow rate, and c) voltage-flow rate

Conclusions

ASDs (accumulation surface diameter) were investigated for PS, PMMA, and their core-shell fibers at different voltages, distances, and flow rates. It was found that regardless of the polymer type or adjusted processing parameters, ASD follows a natural log pattern with time, ending in a plateau. The ASD values and growth rates were compared and discussed. The processing parameter's effect on the ASD and PMMA electrospun fiber diameter was investigated using designed experiments in a response surface-central composite design. For each response, a polynomial model was fitted, and after their diagnostic plots, R^2 and P-values in ANOVA results were evaluated. At higher voltages and distances, ASDs increased, and electrospun fiber diameters would be smaller if the voltages increased while the distance was kept short.

Funding

This research did not receive any specific grant from funding agencies in the public, commercial, or not-for-profit sectors.

References

[1]. Rahmani S., Rafizadeh M., Afshar Taromi F. *J Appl Polym Sci*., 2014, **131:**41179 [Crossref], [Google Scholar], [Publisher]

[2]. Rahmani S., Arefazar A., Latifi M. *Materials Research Express*, 2017, **4**:035304 [Crossref], [Google Scholar], [Publisher]

[3]. Memarian F., Rahmani S., Yousefzadeh M., Latifi M. *Materials in Sports Equipment: Elsevier*, 2019, 123 [Crossref], [Google Scholar], [Publisher]

[4]. Rahmani S., Rafizadeh M. *The Journal of The Textile Institute*, 2017, **108**:2147 [Crossref], [Google Scholar], [Publisher]

[5]. Rahmani S., Arefazar A., Latifi M. *Materials Research Express*, 2017, **4**:085024 [Crossref], [Google Scholar], [Publisher]

[6]. Rahmani S., Maroufkhani M., Mohammadzadeh-Komuleh S., Khoubi-Arani Z. *Fundamentals of Bionanomaterials: Elsevier*, 2022, 175 [Crossref], [Google Scholar], [Publisher]

[7]. Rahmani S., Khoubi-Arani Z., Mohammadzadeh-Komuleh S., Maroufkhani M. *Handbook of Nanocelluloses*, 2021, 1 [Crossref], [Google Scholar], [Publisher]

[8]. Zafar M., Najeeb S., Khurshid Z., Vazirzadeh M., Zohaib S., Najeeb B., Sefat F. *Materials*, 2016, **9**:73 [Crossref], [Google Scholar], [Publisher]

[9]. Theron S., Zussman E., Yarin A. *Polymer*, 2004, **45**:2017 [Crossref], [Google Scholar], [Publisher]
[10]. Uematsu I., Uchida K., Nakagawa Y., Matsumoto H. *Industrial & Engineering Chemistry Research*, 2018, **57**:12122 [Crossref], [Google Scholar], [Publisher]
[11]. Wang C., Hashimoto T., Wang Y. *Macromolecules*, 2021, **54**:7193 [Crossref], [Google Scholar], [Publisher]
[12]. Wang Y., Wang C. *Polymer*, 2021, **22**:2123672 [Crossref], [Google Scholar], [Publisher]
[13]. Lei S., Quan Z., Qin X., Yu J. *Polymer*, 2021, **217**:123456 [Crossref], [Google Scholar], [Publisher]
[14]. B. Sundaray, Babu V.J., Subramanian V., Natarajan T. *Journal of Engineered Fibers and Fabrics*, 2008, **3**:39 [Crossref], [Google Scholar], [Publisher]
[15]. Carrizales C., Pelfrey S., Rincon R., Eubanks T.M., Kuang A., McClure M.J., Bowlin G.L., Macossay J. *Polymers for Advanced Technologies*, 2008, **19**:124 [Crossref], [Google Scholar], [Publisher]
[16]. Liu Y., Ji Y., Ghosh K., Clark R.A., Huang L., Rafailovich M.H. *Journal of Biomedical Materials Research*, 2009, **90A**:1092 [Crossref], [Google Scholar], [Publisher]
[17]. Li L., Jiang Z., Li M., Li R., Fang T., *Rsc Advances.*, 2014, **4**:52973 [Crossref], [Google Scholar], [Publisher]
[18]. Piperno S., Lozzi L., Rastelli R., Passacantando M., Santucci S. *Appl Surf Sci*. 2006, **252**:5583 [Crossref], [Google Scholar], [Publisher]
[19]. Sundaray B., Subramanian V., Natarajan T., Krishnamurthy K. *Appl. Phys. Lett.*, 2006, **88**:143114 [Crossref], [Google Scholar], [Publisher]
[20]. Dong H., Strawhecker K.E., Snyder J.F., Orlicki J.A., Reiner R.S., Rudie A.W. *Carbohydrate Polymers.*, 2012, **87**:2488 [Crossref], [Google Scholar], [Publisher]
[21]. Liu L.Q., Tasis D., Prato M., Wagner H.D., *Advanced Materials*, 2007, **19**:1228 [Crossref], [Google Scholar], [Publisher]
[22]. Liu J., Rasheed A., Dong H., Carr W.W., Dadmun M.D., Kumar S. *Macromol Chem Phys.*, 2008, **209**:2390 [Crossref], [Google Scholar], [Publisher]
[23]. Bedi J.S., Lester D.W., Fang Y.X., Turner J.F., Zhou J., Alfadul S.M., Perry C., Chen Q. *J Polym Eng.*, 2013, **33**:453 [Crossref], [Google Scholar], [Publisher]
[24]. Gupta P., Elkins C., Long T.E., Wilkes G.L. *Polymer*, 2005, **46**:4799 [Crossref], [Google Scholar], [Publisher]
[25]. Mohammad Khanlou H., Chin Ang B., Talebian S., Muhammad Afifi A., Andriyana A. *Textile Research Journal.*, 2015, **85**:356 [Crossref], [Google Scholar], [Publisher]
[26]. Macossay J., Marruffo A., Rincon R., Eubanks T., Kuang A. *Polymers for Advanced Technologies*, 2007, **18**:180 [Crossref], [Google Scholar], [Publisher]
[27]. Khanlou H.M., Sadollah A., Ang B.C., Kim J.H., Talebian S., Ghadimi A. *Neural Computing and Applications*, 2014, **25**:767 [Crossref], [Google Scholar], [Publisher]
[28]. Wang H., Liu Q., Yang Q., Li Y., Wang W., Sun L., Zhang C., Li Y. *Journal of Materials Science*, 2010, **45**:1032 [Crossref], [Google Scholar], [Publisher]

How to cite this manuscript: Shahrzad Rahmani*. Accumulated surface on stationary target: A new approach in electrospinning jet bending instability studies. *Journal of Medicinal and Nanomaterials Chemistry*, 4(3) 2022, 185-195. DOI: 10.48309/JMNC.2022.3.2